All-optical production of ^{6}Li molecular Bose-Einstein condensates in excited hyperfine levels

Yun Long, Feng Xiong, Vinod Gaire, Cameron Caligan, and Colin V. Parker*
School of Physics, Georgia Institute of Technology, 837 State Street NW, Atlanta, Georgia 30332, USA

(Received 20 August 2018; published 29 October 2018)

We present an all-optical method for achieving molecular Bose-Einstein condensates of ^{6}Li. We demonstrate this with mixtures in the lowest two (1-2), and second lowest two (2-3) hyperfine states. For the 1-2 mixture, we can achieve condensate fractions of 36%, with 9×10^4 atoms at 0.05 μK temperature. For the 2-3 mixture, we have 28% condensed with 3.2×10^4 atoms at 0.05 μK temperature. We use mostly standard methods, but make a number of refinements in the magnetic bias coils compared with earlier work. Our method imposes minimal constraints on subsequent experiments by allowing plenty of optical access while requiring only one high-vacuum chamber. We use an optical system designed around minimizing the number of active elements, and we can accomplish slowing and sub-Doppler cooling with a single tapered amplifier.

DOI: 10.1103/PhysRevA.98.043626

I. INTRODUCTION

Since the advent of laser cooling and the formation of the first Bose-Einstein condensates (BECs), the notion of using cold atoms for quantum simulation has been extensively developed and employed [1,2]. Of particular interest to simulating material systems are cold fermionic atoms, which nicely map onto the conduction electrons responsible for many material properties. One interesting system to study is the so-called "BEC-BCS crossover," which occurs when the scattering length between two fermionic spin states diverges [3,4]. For cold atoms, the scattering length can be conveniently tuned to this point using Fano-Feshbach resonances [5–7]. For a many-body system, however, there is in principle a dependence on details of the interaction potential beyond those that determine two-body scattering properties, and beyond two-body corrections to many-body behavior may exist [8,9]. These possibly subtle effects might be isolated more easily if one could control for the two-body effects. To this end, different combinations of hyperfine states of ^{6}Li could be tuned to have nearly identical two-body scattering properties (because the effective range is nearly constant with field [10]) and experience otherwise nearly identical trapping conditions. Thus any difference in many-body behavior could be attributed to beyond two-body effects.

In order to perform these studies, a method is needed to cool and trap the atoms in the appropriate spin states, which ideally would impose minimal constraints on subsequent experiments. Here we demonstrate a method to achieve quantum degeneracy, observed as the formation of a molecular BEC of ^{6}Li, in two combinations of hyperfine states: the lowest two (i.e., 1 and 2 numbering from the bottom) or the second lowest two (i.e., 2 and 3). The apparatus is all-optical, in the sense of using no magnetic trapping potentials. Many all-optical setups exist for the production of degenerate ^{6}Li gases [11–14], including 1-2 and 1-3 [15] hyperfine mixtures. However, our report presents a condensate in the 2-3 hyperfine combination, and combines several attractive features: the condensate is located in a stainless-steel chamber that offers durability and tolerance for thermal gradients, but our design preserves a high degree of optical access: four each of 64- and 38-mm-diameter viewports in the optical table plane, two viewports of 64 mm diameter on the perpendicular axis, and a further 16 viewports of 19 mm diameter at a 21° angle to the optical table. We furthermore use only five active optical sources: two external cavity diode lasers, one Fabry-Perot diode, one tapered amplifier, and one high power fiber laser.

II. APPARATUS

Our system consists of the following components, centered around a large stainless-steel vacuum chamber:

(i) a lithium oven, connected by a Zeeman slower;

(ii) a pair of Bitter-type electromagnets, and three smaller shim coil pairs;

(iii) an *in vacuo* radio-frequency antenna to drive hyperfine transitions;

(iv) a 671-nm amplified laser source, capable of quickly switching between the $D2$ ($^2S_{1/2} \rightarrow {}^2P_{3/2}$) and $D1$ ($^2S_{1/2} \rightarrow {}^2P_{1/2}$) transitions of ^{6}Li;

(v) a high power (200 W) Yb fiber laser with wavelength 1070 nm for far-off-resonant trapping;

(vi) a customized electronic control system built around individual microcontroller units (MCUs).

Figure 1 shows an overview of the main elements of the system. We describe each element in turn.

A. Oven and Zeeman slower

The oven consists of a vertically oriented stainless-steel capped tube and a right-angle elbow, connected to a flange with a triangular orifice filled with microtubes in a hexagonal arrangement, following the design of Ref. [16]. The side length of the triangle is 6.4 mm and the tubes are 5.1 mm long with an outer (inner) diameter of 0.20 (0.10) mm, for an aspect

*cparker@gatech.edu

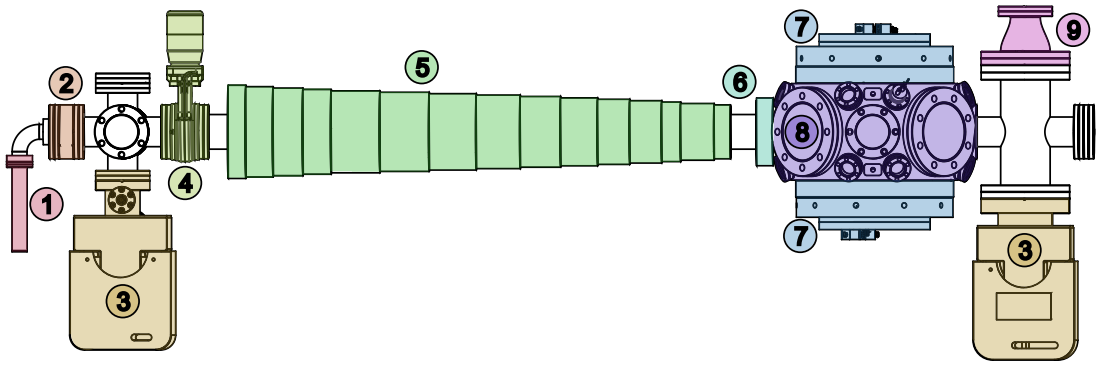

FIG. 1. The main elements of the apparatus: (1) lithium oven, (2) oven flange, (3) ion pumps, (4) oven isolation gate valve, (5) main Zeeman slower section, (6) inverted Zeeman slower section, (7) main magnetic field coils, (8) main chamber, (9) nonevaporable getter. The laser system and shim coils are not shown.

ratio of 50 : 1. The oven is filled with approximately 5 g of enriched ^{6}Li heated to 670–700 K by fiberglass rope heaters driven by a variable autotransformer.

Following the oven, the collimated atomic beam enters a cross-beam spectroscopy chamber, and subsequently the Zeeman slower. The Zeeman slower is of the zero crossing type, and consists of two coil sections, the main coil section being 644 mm long and approximately conical, while the inverted section is a 21-mm-long cylinder. The main section consists of four layers wound directly onto an extended stainless-steel nipple: an inner layer of 6.4 mm outside diameter copper tubing for cooling water, wound in a helix with approximately 25 mm pitch, a second layer of copper sheet covering the tube, a variable thickness of enameled square cross-section copper wire, and another outer helix of cooling tube. The windings are held together with epoxy. The inverted section is fixed to copper fins, which mount to the main section for support and thermal regulation. The coil was designed to produce a square-root field profile, starting from a peak field of 80 mT, and crossing zero to −5 mT. The Zeeman slower exits into the main vacuum chamber, where a magneto-optical trap (MOT) is loaded. The viewport opposite the Zeeman slower is heated to 370 K to reduce accumulation of lithium metal.

B. Magnetic-field control

A moderately large field of 83.2 mT is needed to reach the Feshbach resonance, where the scattering length of ^{6}Li in the lowest two hyperfine states diverges. To provide this, we employ a pair of electromagnets based on a modified Bitter-type design [17]. The basic configuration is a stack of "C" shaped copper pieces, which connect at the ends to the neighboring layers. The pieces are clamped to a mounting plate using bolts. The oversize bolt holes allow cooling water to flow around the bolt, and between the layers guided by gaskets. Unlike Ref. [17], however, our coils consist of two concentric sections, such that the current path is in one end on the inner section, helically through the inner section, between the inner and outer sections at the opposite end, and back helically through the outer section to the starting end (or vice versa). This increases the field for a given current flow, allowing the coils to separate further and increasing optical access to the chamber. The concentric coil design also allows one end of the coil to sit in a reentrant viewport, without the need to use one of the retaining bolts to conduct current, and ensures that the full voltage drop of the coil does not fall between the conducting bolt and the last coil. The latter has been observed to lead to corrosion during inductive voltage spikes in previous designs.

The magnetic environment in the main chamber is additionally controlled by three pairs of independent "shim" coils. The shim coils are circular windings with 25 turns each using the same wire as detailed above for the Zeeman slower. The three pairs have mutually orthogonal axes, with one pair vertically oriented and spaced 125 mm from the chamber, and the other two pairs at 45° to the Zeeman slower axis and spaced 250 mm from the chamber.

Radio-frequency magnetic fields can be applied to the atoms through an *in vacuo* antenna. The antenna is a single, rectangular turn of round cross-section bare copper, perpendicular to both the Zeeman slower and main coil axes, in order to drive $m_F = \pm 1$ transitions. The wire diameter is 1.6 mm, and the rectangle is 64 mm by 38 mm. The antenna was present during the vacuum system bakeout to ensure that outgassing in close proximity to the atomic gas does not reduce the vacuum lifetime.

C. Light sources

The 671-nm source is capable of supplying light at frequencies matching either the $D2$ ($^2S_{1/2} \rightarrow {}^2P_{3/2}$) or $D1$ ($^2S_{1/2} \rightarrow {}^2P_{1/2}$) transitions. Figure 2 shows a schematic of this laser system. Two separate seed sources are derived from external cavity diode lasers (ECDLs), providing about 20 mW of light each. One seed source is locked using a lithium vapor cell [18]. The vapor cell consists of a vacuum "tee" with one arm extended to 500 mm length. In the long arm is placed a chunk of enriched ^{6}Li metal and stainless-steel mesh to help retain the liquid lithium. The cell is heated to 620 K and contains argon buffer gas at approximately 0.1 mbar. The laser is then locked to the $D1$ frequency using the dichroic atomic vapor laser lock (DAVLL) method.

The other ECDL operates at the $D2$ frequency, and is combined with the $D1$ laser to produce a beat note of approximately 10 GHz, which is locked to a microwave source referenced to a commercial rubidium frequency standard. This

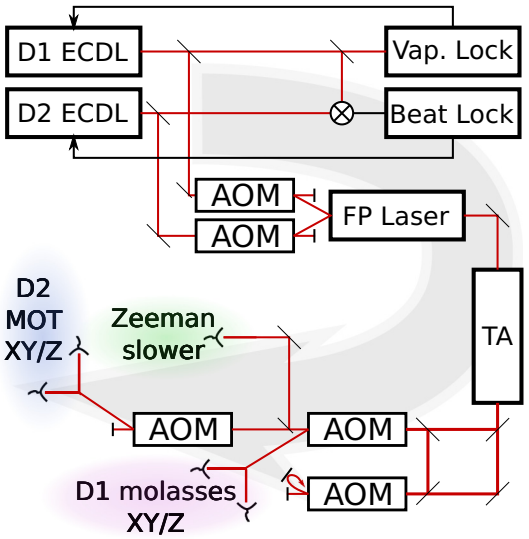

FIG. 2. 671-nm laser system. The system operates at either the $D1$ or $D2$ transitions, using only four active optical elements. Some additional light is taken from the $D2$ laser to provide absorption imaging or optical pumping (not shown). All of the light is fiber coupled before forming the MOT or molasses.

locking method allows the $D2$ frequency to be increased by several GHz as needed to image the atoms in high magnetic fields. A few mW of both the $D1$ and $D2$ light is fed through acousto-optical modulators (AOMs) and through a fiber to the Fabry-Perot (FP) diode laser. This laser is injection-locked to either the $D1$ or $D2$ frequency as needed. The seed source can be switched via the AOMs simultaneously with a change of current. We have found that by providing a step change to the current, together with an exponentially damped component, we can re-establish injection locking after 0.1 ms during the switch.

The injection locked source (about 40 mW total) is then fiber coupled and used as seed light for a tapered amplifier (TA). The benefit of this approach is that even if the original seed AOMs are both left off, the free running FP laser will still seed the TA. The resulting amplified light is about 400 mW total, and is split, with one portion shifted by 228 MHz in order to serve as the repumper for the Zeeman slower or MOT, or as one component of the gray molasses. This light is then mixed back into the original through a polarizing beam splitter (PBS), so that the two components have orthogonal polarizations. When operating for gray molasses, an AOM shifts the light onto the gray molasses path, where it is split evenly to an in-plane (XY) and vertical (Z) component. This splitting also conveniently restores the same polarization state to both frequency components. When operating for a MOT, the first AOM is not used, and the resulting zero order beam is then split evenly to produce the Zeeman slower and MOT light, with the latter passed through an amplitude control AOM and split again into XY and Z paths. Again the even splitting ensures the same polarization state of all components.

The 1070-nm source is an ytterbium-doped fiber laser with unpolarized CW output of 200 W. The source is split by a PBS to yield two polarized sources of approximately 100 W each. Each is passed through an AOM, and subsequently focused into the cell, before exiting to water-cooled beam dumps.

D. Control system

The signals to control the apparatus are generated by a modular system, with each module dedicated to a specific type of output, similar to Ref. [19]. Each module is independent and driven by its own microcontroller unit (MCU). Five types of modules are used, depending on the type of signal needed: parallel digital, serial digital (UART), analog, radio frequency (rf), and microwave (MW). The MCUs can generate the digital signals directly, the other signals are generated by off-the-shelf evaluation boards: 16-bit digital to analog converters (DACs) for analog, direct digital synthesizers (DDSs) for rf (0.1–200 MHz), and phase-locked loop stabilized voltage controlled oscillators (PLLVCOs) for microwave (up to 6.8 GHz). All of the modules are connected to a common 50-kHz clock, a synchronization signal, and a master MCU. The master MCU subsequently communicates by ethernet with the host computer. This obviates the need for ethernet-capable MCUs in each module as in previous designs [19]. A further unique element of our design is that all modules generate their response on-the-fly, that is, the entire sequence does not need to be precomputed. Most commonly this is used to reduce bandwidth by specifying only ramp endpoints, but it can also be used to feedback stabilize an output, as the MCUs have built-in analog-to-digital converters (ADCs).

III. MAGNETO-OPTICAL TRAP (MOT)

The ^{6}Li atoms are precooled by a Zeeman slower and collected by the magneto-optic trap (MOT) with a standard three-retroreflected beams configuration. Following a MOT load phase, we compress the MOT, after which we further cool the atoms to below the Doppler limit by $D1$ gray molasses (see below). The optical levels used and relevant detunings are labeled in Fig. 2. The Zeeman slower beam is 80 mW, with 138 MHz red detuning from the $D2$ cooling transition for the main component, with approximately 20% of the light as repumper. The diameter is about 15 mm at the entrance and slightly converges to match the expanding atomic beam through the slower. The horizontal MOT beams have 40 mm diameter and the vertical beams have 20 mm diameter. During loading, the cooling light is 43 MHz red detuned from the $D2$ cooling transition ($F = 3/2 \rightarrow F'$) with 20 mW in each beam, and the repumping beams are 38 MHz red detuned from the repumping transition ($F = 1/2 \rightarrow F'$) with a power of 4 mW in each beam (see Fig. 3). We at best have 1.2×10^9 atoms in the MOT after 10 s loading. We compress the MOT (known as CMOT) by increasing the gradient from 160 to 480 μT/mm, simultaneously shifting the cooling and repumping light 20 MHz closer to the transition frequency, while the cooling and repumping powers decrease to 9.1% and 3.2% of their previous values, respectively.

IV. GRAY MOLASSES

To get a better initial phase space density (PSD) for evaporation, we use $D1$ gray molasses cooling before loading

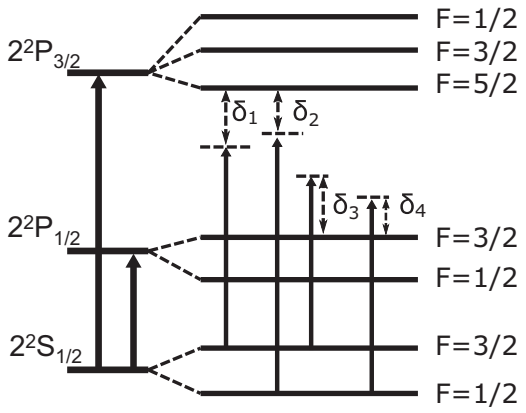

FIG. 3. The hyperfine structure of ground and low excited states of ^{6}Li. The experimentally optimized detuning values are $\delta_1 = -43$ MHz (MOT), $\delta_2 = -38$ MHz (MOT repumper), $\delta_3 = \delta_4 = 32$ MHz (gray molasses).

atoms into our dipole trap. The $D1$ gray molasses cooling is a very effective sub-Doppler cooling method for lithium that relies on interference between two components of light with a relative frequency difference matched to the ground-state hyperfine levels [13,20–22]. Our molasses beams share windows with the MOT beams but have small beam diameters of 11 mm for the horizontal direction and 8 mm for the vertical direction. The total power is 137 mW with a fraction of 5% of repumper. In order to optimize the captured fraction and the final temperature, we employ a two-stage procedure. The first stage begins after quickly switching off the CMOT gradient and $D2$ cooling beams, and lasts about 5 ms. The total $D1$ light intensity is 400 mW/cm^2. The second stage lasts only 0.2 ms, during which the AOM is ramped down to produce 25% of the starting intensity. The effectiveness of $D1$ gray molasses is quite sensitive to the two-photon detuning, which is precisely controlled by an AOM. We plot the temperature against two photon detuning in Fig. 4. The $D1$ gray molasses, like other sub-Doppler schemes, is sensitive

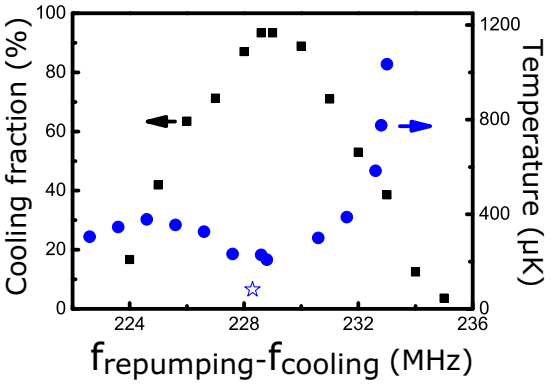

FIG. 4. Cooling fraction (black squares) and temperature (blue circles) after two stage $D1$ molasses cooling without canceling stray field (we estimate the field to be 300 mG). The cooling is only a small improvement, but the frequency sensitivity shows that the gray molasses cooling mechanism is working. After canceling the residual field to better than 10 mG, the temperature dropped dramatically to 80 μK (blue star).

to residual magnetic fields, so we zero the main coil current and use the shim coils to cancel the residual field. Although careful field cancellation was necessary to achieve significant temperature reduction, all of the other conditions could be optimized under larger stray field conditions. The residual field cancellation was adjusted and verified by measuring radio-frequency transitions between hyperfine states. Somewhat surprisingly given the extreme sensitivity, we were not successful in using the cooling efficacy alone to find the zero-field condition. Under optimal conditions, we have close to 100% of the atoms cooled and the temperature reduced to 80 μK. Since the single photon detuning isn't critical to the $D1$ gray molasses, the light shift from the dipole laser is not harmful and we increase the optical dipole power during the $D1$ molasses. At the end of $D1$ molasses cooling, we shut off the repumper 0.1 ms before the cooling beam, so the atoms are optically pumped into the lowest two hyperfine states.

V. EVAPORATION AND BEC

In what follows we label the absolute lowest three hyperfine levels as $|1\rangle$, $|2\rangle$, and $|3\rangle$, in increasing order of energy. These are adiabatically connected to the levels $|m_s, m_I\rangle = |-1/2, 1\rangle$, $|-1/2, 0\rangle$, and $|-1/2, -1\rangle$, respectively, at high field. The evaporation starts with loading a $|1\rangle$ and $2\rangle$ mixture into a crossed optical dipole trap. This hyperfine population results from turning off the component of light near the $F = 1/2$ transition at the end of the molasses phase. The dipole trap is formed by two beams of 1070 nm light intersecting at 13° on the atomic cloud. Each beam has a maximum 65 W power with a waist of 32 μm. The power is controlled by an AOM, to which we apply a 1-MHz frequency modulation to extend the trap volume at the early stages of evaporation. The laser power ramps up in 2 ms to its maximum during the CMOT phase. The magnetic field ramps up to 79.0 mT in 60 ms after $D1$ gray molasses cooling. The laser power remains constant 10 ms after the field ramp up finishes. At this point about 2.5×10^6 atoms of each spin state are loaded into the dipole trap and the experiment is ready for forced evaporation.

We have made molecular Bose-Einstein condensates in both $|1\rangle$-$|2\rangle$ and $|2\rangle$-$|3\rangle$ mixtures. In order to make a $|1\rangle$-$|2\rangle$ molecular BEC, we use forced evaporation. The first stage of evaporation lasts 700 ms, during which we ramp down the laser power to decrease the temperature, and the magnetic field shifts to 75.1 mT for a convenient binding energy to generate Feshbach molecules. We confirm the existence of molecules by radio-frequency spectroscopy between the $|2\rangle$ and $|3\rangle$ states as shown in Fig. 5. The binding energy can be estimated by the formula $E_B/k_B = \hbar^2/(ma^2k_B) = 2.2$ μK, where E_B is the binding energy and $a = 188$ nm at 75.1 mT is the s-wave scattering length [7]. We then spend 600 ms to gradually decrease the modulation and increase the atom density, and then a further 800 ms of evaporation before the molecular BEC emerges. The atom number and temperature during evaporation are plotted in Fig. 6.

The bimodal profile is one of the easiest tests for the existence of BEC [23]. However, for ^{6}Li in the strongly interacting region, a special imaging procedure is used to make the profile more obvious [24]. We first ramp down the field from 79.0 to 50.0 mT in 1 ms at the start of the

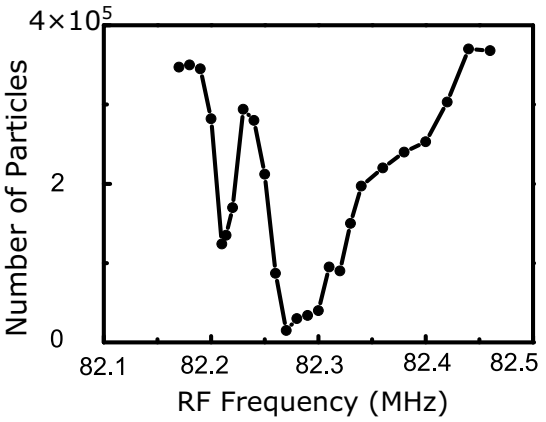

FIG. 5. rf spectroscopy. The left dip is the free-to-free resonance of the $|2\rangle$ to $|3\rangle$ transition, while the right dip is the bound-to-free transition indicating the existence of Feshbach molecules. The frequency difference between these two dips is about 60(10) kHz, close to the binding energy of 2.2 μK by calculation.

time-of-flight, so the molecules can expand ballistically. At this field the binding energy is too deep to image, so we then ramp up to 85.0 mT to unbind the molecules during the second half of the time-of-flight period. This increasing field ramp takes about 5 ms, limited by the coil inductance. Our high-field experiments are greatly aided by the beat lock of the $D2$ laser used for imaging, which allows absorption images at GHz Zeeman shifts. Using this procedure, a clear signature of molecular BEC can be seen at the end of the evaporation (see Fig. 7). We estimate that we can have condensates with nearly 10^5 molecules, about $36 \pm 4\%$ of which are in the BEC. The total number is determined by standard absorption imaging methods, and a bimodal fit is used to estimate condensation fraction. There is some systematic uncertainty to this estimate due to the rapidly changing scattering length during the initial time-of-flight period, which prevents true ballistic expansion. Since these effects cover 1 ms out of the 11 ms time of flight period, we estimate this uncertainty at 10%, comparable to imaging shot-noise uncertainty. Similar considerations apply to the temperature, which is estimated to be around 0.05 μK, based on the thermal portion of the image. At lower laser

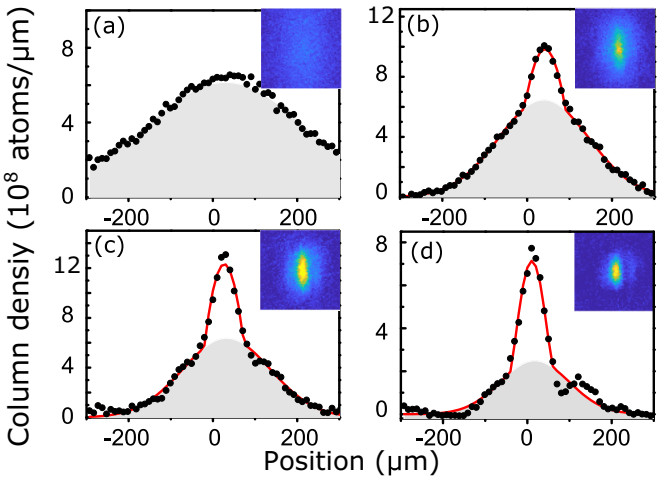

FIG. 7. Bimodel fitting of column density and false color optical density profile after 11-ms ballistic expansion when evaporating a $|1\rangle$-$|2\rangle$ mixture to successively lower dipole laser powers (P). (a) $P = 247$ mW, where temperature is $T = 1.9$ μK, and molecule number $N = 2.7 \times 10^5$. No condensation can be observed. (b) $P = 139$ mW, $T = 0.31$ μK, and $N = 1.9 \times 10^5$. 10% of molecules are condensed. (c) $P = 88$ mW, where $T = 0.06$ μK, and $N = 1.6 \times 10^5$. 19% of molecules are condensed. (d) $P = 57$ mW, where $T = 0.05$ μK, and $N = 9 \times 10^4$. 36% of atoms are condensed. The ideal gas Fermi temperature and BEC critical temperature would be 0.57 and 0.30 μK, respectively, under these conditions. The fits are done using a 2D Gaussian profile plus a truncated elliptic paraboloid.

powers, the temperature does not decrease significantly, suggesting there may be competing heating processes [14].

To make a $|2\rangle$-$|3\rangle$ molecular BEC, we start by loading a $|1\rangle$-$|2\rangle$ mixture into crossed dipole trap. Then, we transfer atoms to the desired spin states, which requires a two-pulse sequence: $|2\rangle \rightarrow |3\rangle$, followed by $|1\rangle \rightarrow |2\rangle$. A challenge to this process are collisions and field inhomogeneity, as both destroy the coherence of the transfer. To avoid collisions, one might like to work around 55.0 mT where scattering cross sections are small. However, at this field the difference of magnetic moment is much larger, and our inhomogeneous field makes such transfers poor. Instead we opt to do fast transfers at 73.6 mT and accept the collisional incoherence.

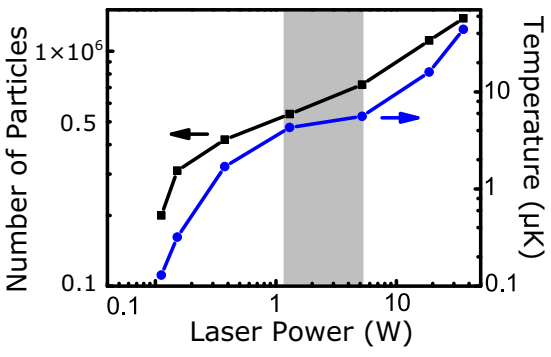

FIG. 6. The atom number and temperature during evaporation for $|1\rangle$-$|2\rangle$ molecular BEC. The gray region indicates where we compress the dipole trap.

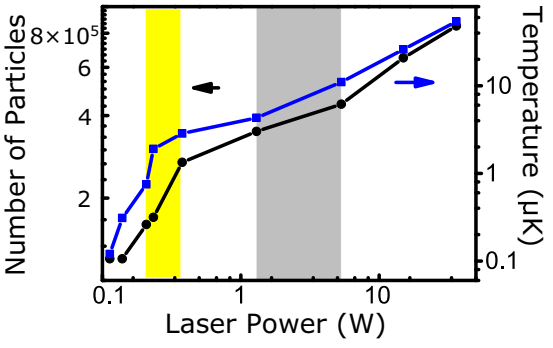

FIG. 8. The atom number and temperature during evaporation for $|2\rangle$-$|3\rangle$ molecular BEC. The gray region indicates we compress the volume of dipole trap. We ramp the magnetic field to increase the binding energy when crossing the yellow region

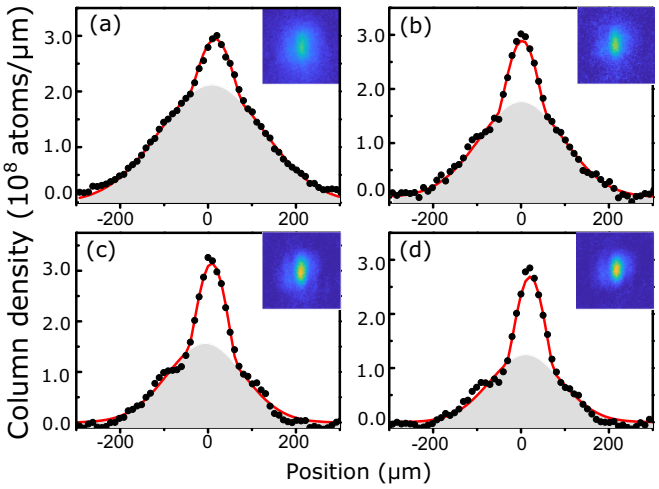

FIG. 9. Bimodal fitting of column density and false color optical density profile after 11-ms ballistic expansion when evaporating a $|2\rangle$-$|3\rangle$ mixture to successively lower dipole laser powers (P). (a) $P = 112$ mW, where temperature $T = 0.13$ μK, and molecule number $N = 8.1 \times 10^4$. 9% of molecules are condensed. (b) $P = 104$ mW, where $T = 0.12$ μK, and $N = 6.1 \times 10^4$. 16% of molecules are condensed. (c) $P = 88$ mW, where $T = 0.06$ μK, and $N = 4.8 \times 10^4$. 23% of molecules are condensed. (d) $P = 68$ mW, where $T = 0.05$ μK, and $N = 3.2 \times 10^4$. 28% of molecules are condensed. The ideal gas Fermi temperature and BEC critical temperature would be 0.44 and 0.23 μK, respectively, under these conditions. The fits are done using a 2D Gaussian profile plus a truncated elliptic paraboloid. Each image shown is the average of five acquisitions.

We apply a 0.36-ms π pulse to transfer the atoms from $|2\rangle$ to $|3\rangle$ and then a 0.48-ms π pulse to transfer the atoms from $|1\rangle$ to $|2\rangle$. About 50% of the atoms can be successfully driven to $|3\rangle$ by the first pulse. We believe the efficiency is limited by the decoherence due to the existence of $|1\rangle$. The transfer efficiency of our π pulse can be as high as 80% when no $|1\rangle$ atoms exist, and Landau-Zener sweeps have similar performance. The imperfect transfer here is most likely due to the curvature of the magnetic field. Currently we limit the rf power to 2 W, so coherence may improve with faster transfers and shorter pulse times. A light pulse resonant with state $|1\rangle$ clears the residual atoms right after the second rf pulse to avoid depletion due to inelastic collisions. We have about 1×10^6 $|2\rangle$ atoms and 8×10^5 $|3\rangle$ atoms remaining in the trap with a temperature of 54 μK. We evaporate the $|2\rangle$-$|3\rangle$ mixture at 75.7 mT to 11 μK in 200 ms. Then we decrease the modulation of the AOM to compress the dipole trap within 400 ms. After that during the next 600 ms of evaporation we ramp the field to 74.2 mT where we expected the $|2\rangle$-$|3\rangle$ binding energy is similar to $|1\rangle$-$|2\rangle$ mixture at 75.1 mT. The binding energy is 80 kHz as measured with the same rf transfer method used for the $|1\rangle$-$|2\rangle$ mixture. We observe the BEC by applying a further 700-ms evaporation. The atom number and temperature during evaporation are shown in Fig. 8. We use the same imaging technique to identify the bimodal distribution and determine the BEC condensate fraction as shown in Fig. 9. At best we can have $28 \pm 3\%$ atoms condensed with a total number of 3.2×10^4. Although the rf transfer incurs a significant atom number loss, we can see that it does not prevent the formation of condensates.

VI. CONCLUSION

In conclusion, we have demonstrated an all-optical method for producing molecular BECs of ^{6}Li in either the $|1\rangle$-$|2\rangle$ or $|2\rangle$-$|3\rangle$ hyperfine mixtures. In principle it would be easy to extend this to the $|1\rangle$-$|3\rangle$ mixture as well. These experiments pave the way for future investigations of degenerate Fermi gases and detailed comparisons of many-body properties between mixtures with identical two-body collisional properties.

ACKNOWLEDGMENT

We acknowledge support from the Air Force Office of Scientific Research, Young Investigator Program, through Grant No. FA9550-18-1-0047.

[1] I. Bloch, J. Dalibard, and W. Zwerger, Rev. Mod. Phys. **80**, 885 (2008).
[2] I. M. Georgescu, S. Ashhab, and F. Nori, Rev. Mod. Phys. **86**, 153 (2014).
[3] M. Bartenstein, A. Altmeyer, S. Riedl, S. Jochim, C. Chin, J. H. Denschlag, and R. Grimm, Phys. Rev. Lett. **92**, 120401 (2004).
[4] M. Randeria and E. Taylor, Annu. Rev. Condens. Matter Phys. **5**, 209 (2014).
[5] E. Tiesinga, B. J. Verhaar, and H. T. C. Stoof, Phys. Rev. A **47**, 4114 (1993).
[6] S. Inouye, M. R. Andrews, J. Stenger, H. J. Miesner, D. M. Stamper-Kurn, and W. Ketterle, Nature (London) **392**, 151 (1998).
[7] C. Chin, R. Grimm, P. Julienne, and E. Tiesinga, Rev. Mod. Phys. **82**, 1225 (2010).
[8] S. Tan, Phys. Rev. A **78**, 013636 (2008).
[9] S. Zhu and S. Tan, arXiv:1710.04147.
[10] P. Naidon and M. Ueda, C. R. Phys. **12**, 13 (2011).
[11] K. M. O'Hara, S. L. Hemmer, M. E. Gehm, S. R. Granade, and J. E. Thomas, Science **298**, 2179 (2002).
[12] S. Jochim, M. Bartenstein, A. Altmeyer, G. Hendl, S. Riedl, C. Chin, J. H. Denschlag, and R. Grimm, Science **302**, 2101 (2003).
[13] A. Burchianti, G. Valtolina, J. A. Seman, E. Pace, M. De Pas, M. Inguscio, M. Zaccanti, and G. Roati, Phys. Rev. A **90**, 043408 (2014).
[14] S.-J. Deng, P.-P. Diao, Q.-L. Yu, and H.-B. Wu, Chin. Phys. Lett. **32**, 053401 (2015).
[15] P. A. Murthy, M. Neidig, R. Klemt, L. Bayha, I. Boettcher, T. Enss, M. Holten, G. Zürn, P. M. Preiss, and S. Jochim, Science **359**, 452 (2018).

[16] R. Senaratne, S. V. Rajagopal, Z. A. Geiger, K. M. Fujiwara, V. Lebedev, and D. M. Weld, Rev. Sci. Instrum. **86**, 023105 (2015).
[17] D. O. Sabulsky, C. V. Parker, N. D. Gemelke, and C. Chin, Rev. Sci. Instrum. **84**, 104706 (2013).
[18] N. Ohtsubo, T. Aoki, and Y. Torii, Opt. Lett. **37**, 2865 (2012).
[19] P. E. Gaskell, J. J. Thorn, S. Alba, and D. A. Steck, Rev. Sci. Instrum. **80**, 115103 (2009).
[20] D. R. Fernandes, F. Sievers, N. Kretzschmar, S. Wu, C. Salomon, and F. Chevy, Europhys. Lett. **100**, 63001 (2012).
[21] A. T. Grier, I. Ferrier-Barbut, B. S. Rem, M. Delehaye, L. Khaykovich, F. Chevy, and C. Salomon, Phys. Rev. A **87**, 063411 (2013).
[22] F. Sievers, N. Kretzschmar, D. R. Fernandes, D. Suchet, M. Rabinovic, S. Wu, C. V. Parker, L. Khaykovich, C. Salomon, and F. Chevy, Phys. Rev. A **91**, 023426 (2015).
[23] M. W. Zwierlein, C. A. Stan, C. H. Schunck, S. M. F. Raupach, S. Gupta, Z. Hadzibabic, and W. Ketterle, Phys. Rev. Lett. **91**, 250401 (2003).
[24] M. Kohnen, diploma thesis, University of Heidelberg, 2008, http://www.lithium6.de/news/files/diplomarbeit-matthias.pdf.